Title: Psilocybin induces rapid and persistent growth of dendritic spines in frontal cortex *in vivo*

Authors: Ling-Xiao Shao[1], Clara Liao[2], Ian Gregg[1], Neil K. Savalia[3], Kristina Delagarza[1], Alex C. Kwan[1,2,3,4]

[1]Department of Psychiatry,
[2]Interdepartmental Neuroscience Program,
[3]Medical Scientist Training Program,
[4]Department of Neuroscience,
Yale University School of Medicine, New Haven, Connecticut, 06511, USA
Correspondence: alex.kwan@yale.edu

Keywords: dendrites; neural plasticity; structural remodeling; serotonergic psychedelic; hallucinogen; antidepressant

Abstract
Psilocybin is a serotonergic psychedelic with untapped therapeutic potential. Here we chronically imaged apical dendritic spines of layer 5 pyramidal neurons in mouse medial frontal cortex. We found that a single dose of psilocybin led to ~10% increases in spine density and spine head width. Synaptic remodeling occurred quickly within 24 hours and was persistent 1 month later. The results demonstrate structural plasticity that may underpin psilocybin's long-lasting beneficial actions.

Main Text
Serotonergic psychedelics are compounds that produce an atypical state of consciousness characterized by altered perception, cognition, and mood. It has long been recognized that these compounds may have therapeutic potential for neuropsychiatric disorders including depression, obsessive-compulsive disorder, and addiction[1]. Among psychedelics, psilocybin is recently shown to relieve depression symptoms rapidly and with sustained benefits for several months[2, 3]. The therapeutic effects may arise from the ability of psilocybin to induce neural adaptations. The expressions of genes involved in synaptic plasticity are elevated after administration of serotonergic psychedelics in rats[4, 5]. In neuronal cultures, bath application of serotonergic psychedelics induces transient increases in spine size[6] and proliferation of dendritic branches[7]. A recent study showed that an analogue of ibogaine, a psychedelic with differing molecular targets from psilocybin, increases spine formation rate in mice[8]. Thus, there is only limited evidence linking serotonergic psychedelics to structural plasticity *in vivo*. Importantly, the time scale in which synaptic remodeling may occur in the mammalian brain is unknown.

To test the potency and dose dependence of psilocybin in mice, we measured the head-twitch response, a classic assay for characterizing psychedelic compounds in rodents. We observed that mice would exhibit high-frequency headshakes intermittently after administration of psilocybin. We characterized 82 C57BL/6J mice with 5 doses of psilocybin (0, 0.25, 0.5, 1, 2 mg/kg, i.p.; range = 7-10 per sex per dose). A sharp rise of elicited head-twitch responses occurred at 1 mg/kg (**Fig. 1a, b**), consistent with a prior report[9]. Thus, we chose to use 1 mg/kg – the inflection point of the dose-dependence curve – to assess psilocybin's effect on structural plasticity.

In the body, psilocybin is dephosphorylated to psilocin, an agonist of 5-HT_{2A} receptors that are densely expressed in apical dendrites of pyramidal neurons in the medial frontal cortex of primates and rodents[10, 11]. We therefore hypothesize that psilocybin may modify the dendritic architecture in the medial frontal cortex. We used chronic two-photon microscopy to track apical dendritic spines in the cingulate/premotor (Cg1/M2) region of *Thy1*^{GFP} mice, in which a sparse subset of layer 5 pyramidal neurons express GFP[12] (**Fig. 1c, d**). We imaged before and after administering psilocybin (1 mg/kg, i.p.) or saline at 2-day intervals and then again 1 month later for a total of 7 imaging sessions (**Fig. 1e, f**). In total, we tracked 1,820 dendritic spines on 161 branches from 12 animals. Spine morphology was analyzed blind to experimental conditions using standardized procedures[13]. Our results indicate that a single dose of psilocybin induces a significant elevation in spine density (+7±2% on Day 1, +12±3% on Day 7; main effect of treatment, P=0.011, mixed-effects model to account for variations across dendrites and mice; **Fig. 1g–i**) and increase in the width of spine heads (+11±2% on Day 1, and +5±1% on Day 7; main effect of treatment, P=0.013; **Fig. 1j–l, Supplementary Fig. 1**). Details for all statistical tests including sample sizes are provided in **Supplementary Table 1**.

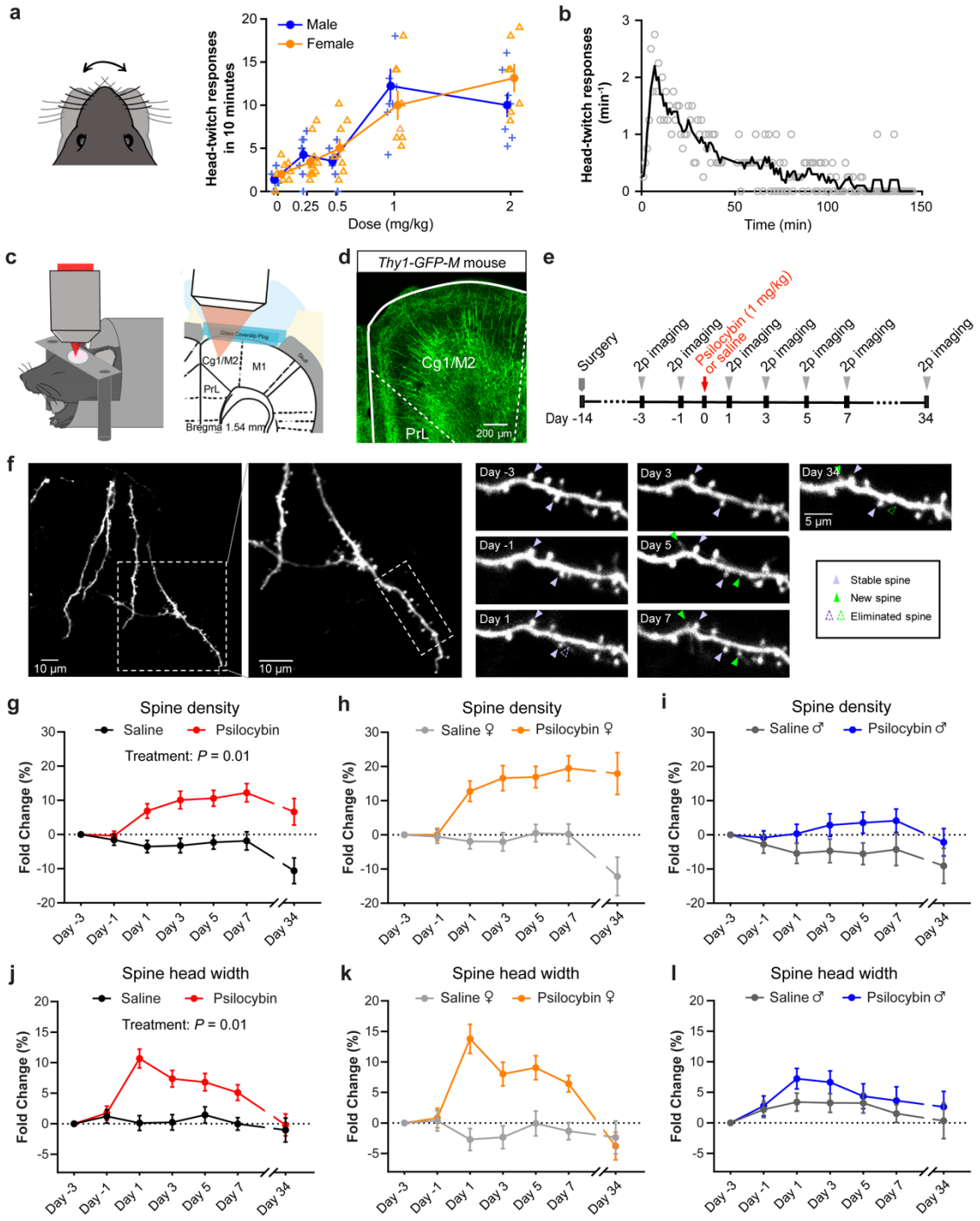

Figure 1: Psilocybin increases the density and size of dendritic spines in the mouse medial frontal cortex. **(a)** Head-twitch responses as a function of dose, tested on 82 C57BL/6J mice. **(b)** Time course of head-twitch responses after administrating psilocybin (1 mg/kg, i.p.), averaged from 2 males and 2 female C57BL/6J mice. Line, moving average. **(c)** Imaging setup. **(d)** Fixed coronal section from *Thy1*^{GFP} mice. **(e)** Timeline of experiment. **(f)** Example field of view. **(g)** Effects of psilocybin or saline treatment on spine density, plotted as fold-change from baseline value on Day -3. Mean ± SEM. **(h, i)** Similar to (g), plotted separately for females and males. **(j – l)** Similar to (g – i) for spine head width. Sample sizes and details of the ANOVA models are provided in Supplementary Table 1.

Increased spine density could be due to higher formation rate, lower elimination rate, or both. To distinguish between the possibilities, we leveraged the longitudinal data set to determine the turnover rates of dendritic spines. In females, the spine formation increased by 8±2% after psilocybin (7±1% on Day -1, 15±2% on Day 1; **Fig. 2a, b**). Likewise, the spine formation rate was higher by 4±2% in males after psilocybin (6±1% on Day -1, 10±2% on Day 1). By contrast, there was no change in the elimination rate of spines (**Fig. 2c**). A key question

was whether the new spines formed after psilocybin administration would persist, because nascent dendritic spines can take 4 days to mature into functional synapses[14]. For this reason, we imaged 34 days after psilocybin administration and observed that a fraction of the psilocybin-induced new spines remained stable (**Fig. 2d**). Altogether, these results demonstrate that a single dose of psilocybin induces rapid and long-lasting dendritic remodeling in layer 5 pyramidal neurons in the mouse medial frontal cortex.

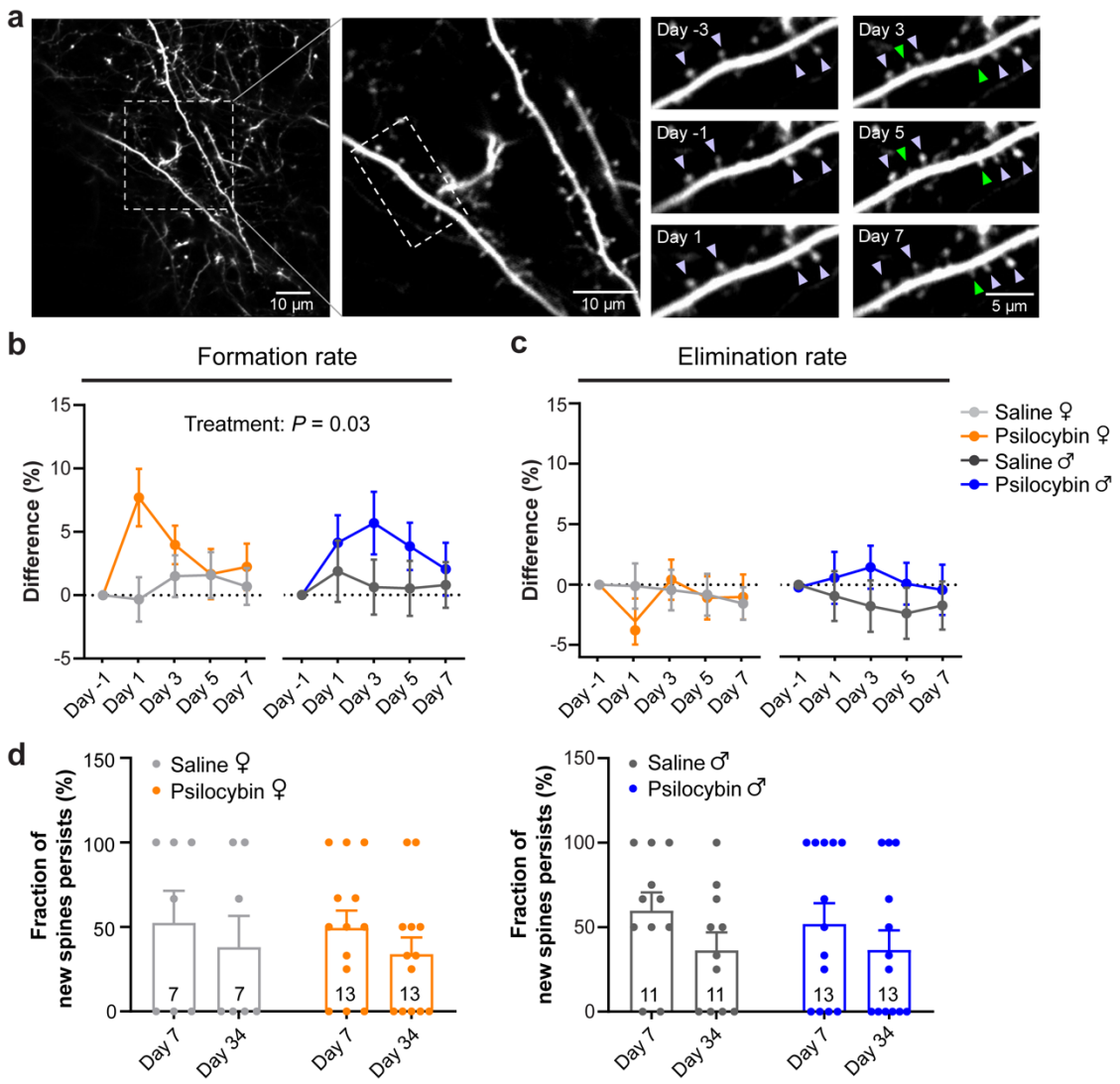

Figure 2. Psilocybin elevates the formation rate of dendritic spines. (a) Example field of view. Purple arrowhead, stable spine. Green arrowhead, new spine. **(b)** Effects of psilocybin or saline treatment on the formation rates of dendritic spines for female and male mice, plotted as difference from baseline value on Day -1. Mean ± SEM. **(c)** Similar to (b) for elimination rates. **(d)** Fraction of spines newly formed on Day 1 that remained stable on Day 7 and Day 34 for female and male mice. Filled circles, individual dendritic segments. Sample sizes and details of the ANOVA models are provided in Supplementary Table 1.

To further support the conclusions, we tried to replicate the findings in another cohort of animals using a different approach. We administered *Thy1*^{GFP} mice with psilocybin (1 mg/kg, i.p.) or saline, sacrificed them 24 hours later, and imaged coronal brain sections using confocal microscopy. We expanded analyses to 6 areas of the brain, including 2 zones that encompass apical and basal dendrites and 3 regions of the frontal cortex: Cg1/M2, prelimbic/infralimbic (PrL/IL), and primary motor cortex (M1) (**Fig. 3a–c**). The results, consisting of 23,226 dendritic spines counted on 1,885 branches from 12 animals, reaffirmed the ability of psilocybin to promote the growth of new dendritic spines in Cg1/M2 in female mice (spine density: 0.46±0.02 versus 0.50 ±0.01 µm^{-1}; **Fig. 3d**). Effects of psilocybin on spine density were more pronounced in female animals (treatment x sex, P = 0.013, two-way ANOVA; **Fig. 3d**), echoing the trend observed in the two-photon imaging data (**Fig. 1h–i, k–l**). We did not detect differences in spine protrusion length and spine head width (**Fig. 3e, f**), which may be due to the across-subjects design, as it has less power than the within-subjects design of the chronic imaging experiment. There were select morphological differences in PrL/IL and M1 (**Fig. 3g–n;**

Supplementary Fig. 2). Psilocybin also had significant impact on basal dendrites in Cg1/M2 (**Fig. 3o–r**). Overall, the two sets of data converge to indicate that psilocybin promotes the rapid growth of new dendritic spines in layer 5 pyramidal neurons in the medial frontal cortex.

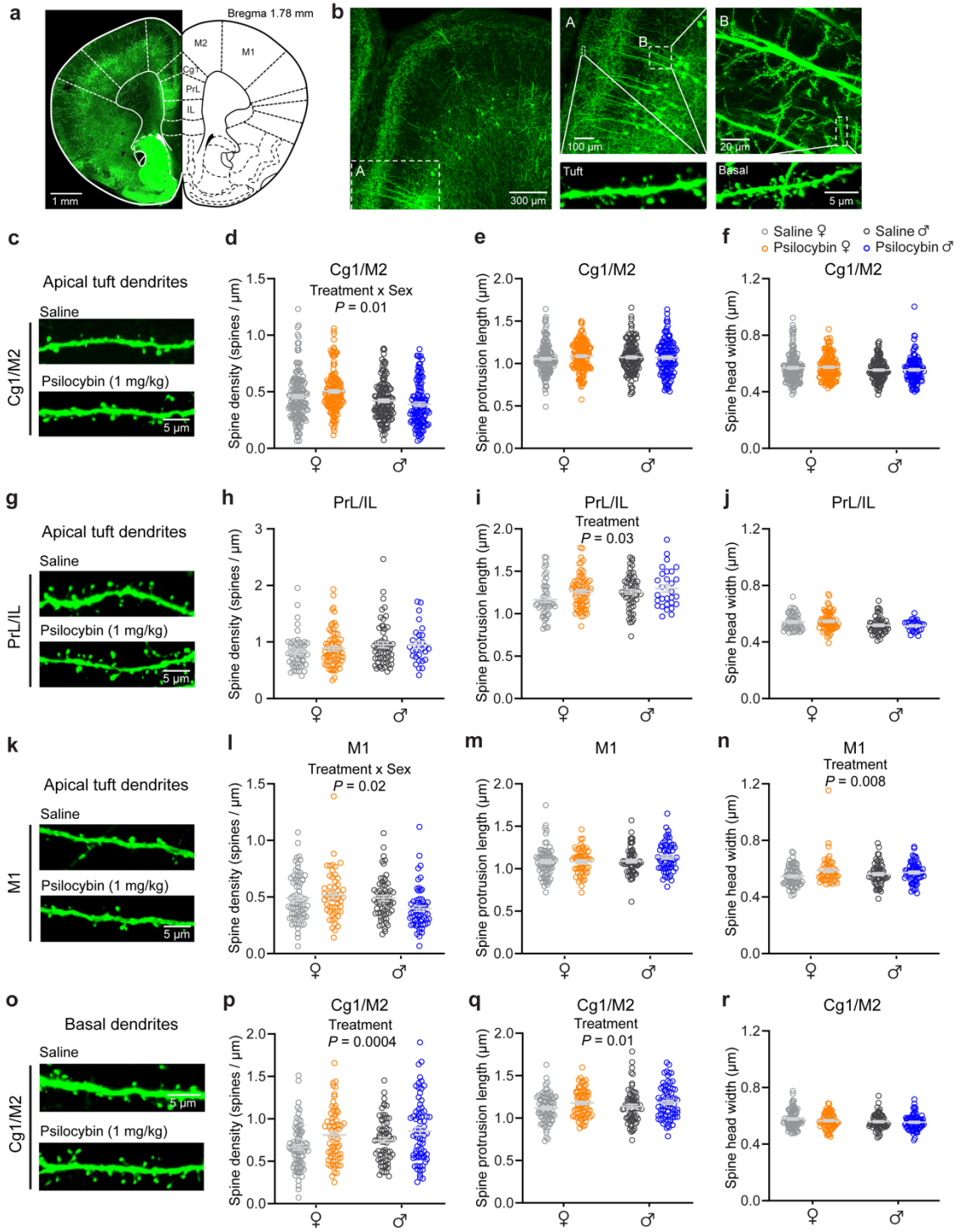

Figure 3. Region-specific effects of psilocybin. (a) Stitched confocal image of a coronal brain section from a *Thy1*^{GFP} mouse. **(b)** Magnified images showing apical and basal dendritic segments. **(c)** Images of apical dendrites in Cg1/M2. **(d)** Effects of psilocybin and saline on spine density for apical dendrites in Cg1/M2. Open circles, individual dendritic segments. Gray line, mean ± SEM. **(e)** Similar to (d) for spine protrusion length. **(f)** Similar to (d) for spine head width. **(g – j)** Similar to (c – f) for PrL/IL. **(k – n)** Similar to (c – f) for M1. **(o – r)** Similar to (c – f) for basal dendrites in Cg1/M2. Sample sizes and details of the ANOVA models are provided in Supplementary Table 1.

The regional specificity of the psilocybin-induced structural plasticity is notable, because prior studies indicated that the cingulate cortex is essential for head-twitch responses in rodents[15]. The colocalization of head-twitch responses (which reflect hallucinogenic potency) and dendritic plasticity (which is typically involved in therapeutic effects) in the same brain region adds to the debate over whether the hallucinogenic effects of serotonergic psychedelics are dissociable from the therapeutic effects[16, 17]. By demonstrating that psilocybin can promote structural plasticity in the mammalian brain *in vivo*, our study suggests that dendritic remodeling may be a mechanism shared by compounds with rapid antidepressant effects. For instance, ketamine similarly increases spine density by elevating spine formation rate in the medial frontal cortex[18, 19]. However, still unknown is how drugs with disparate molecular targets may yield comparable circuit-level modifications[20]. Elucidating the mechanisms will be crucial towards unraveling the neurobiology of rapid-acting antidepressants.

Methods

Animals

All experiments were performed on males and females. *Thy1*^{GFP} (Tg(Thy1-EGFP)MJrs/J, Stock No.007788) transgenic mice and C57BL/6J (Stock No. 000664) mice were obtained from Jackson Laboratory. For head-twitch response, 6 to 10-week-old C57BL/6J mice were used. For two-photon imaging, *Thy1*^{GFP} mice underwent surgery when they were 6 to 8-week-old and then were used for imaging ~2 weeks later. For confocal imaging, 8 to 12-week-old *Thy1*^{GFP} mice were used. Mice were group housed (2 – 5 mice per cage) under controlled temperature in a 12hr light–dark cycle (7:00 AM to 7:00 PM) with free access to food and water. Animal care and experimental procedures were approved by the Institutional Animal Care & Use Committee (IACUC) at Yale University.

Head-twitch response

Head-twitch response was evaluated using 40 male and 42 female C57BL/6J mice. Upon arrival, animals habituated at the housing facility for >2 weeks before behavioral testing. Behavioral testing took place between 10:00 AM and 4:00 PM. Animals were weighed and injected intraperitoneally with saline or psilocybin (0.25, 0.5, 1, or 2 mg/kg). We measured head-twitch response in groups of two animals: after injections, the two animals were immediately placed into separate chambers, made by inserting a plastic divider to halve an open-field-activity box (12” W x 6” H x 10” D). The box was within a sound attenuating cubicle with a built-in near-infrared light source and a white light source (interior: 28” W x 34” H x 22” D, Med Associates Inc.). Videos were recorded by a high-speed (213 fps), near-infrared camera (Genie Nano M1280, Teledyne Dalsa) mounted overhead above the open-field-activity box. Typical recordings were 30 minutes long and, for a subset of mice (2 males and 2 females), extended to >150 minutes. Between each measurement, the open-field activity box was thoroughly cleaned with 70% ethanol. The videos were scored for head twitches by an experienced observer blind to the experimental conditions.

Surgery

Prior to surgery, the mouse was injected with carprofen (5 mg/kg, s.c.; 024751, Henry Schein Animal Health,) and dexamethasone (3 mg/kg, i.m.; 002459, Henry Schein Animal Health). During surgery, the mouse was anesthetized with isoflurane (3 – 4% for induction and 1 – 1.5% for the remainder of surgery) and fixed in a stereotaxic apparatus (David Kopf Instruments). The body of the mouse rested on a water-circulating heating pad (Stryker Corp) set to 38 °C. Petrolatum ophthalmic ointment (Dechra) was used to cover the animal’s eyes. The hair on the head was shaved, and the scalp was wiped and disinfected with ethanol pad and betadine. An incision was made to remove the skin and the connective tissue above the skull was removed. Subsequently, a dental drill was used to make a ~3-mm-diameter circular craniotomy above the right medial frontal cortex (center position: +1.5 mm anterior-posterior, AP; +0.4 mm medial-lateral, ML; relative to bregma). Artificial cerebrospinal fluid (ACSF, containing (in mM): 135 NaCl, 5 HEPES, 5 KCl, 1.8 CaCl2, 1 MgCl2; pH 7.3) was used to irrigate the exposed dura above brain. A two-layer glass window was made from two round 3-mm-diameter, #1 thickness glass coverslip (64-0720 (CS-3R), Warner Instruments), bonded by UV-curing optical adhesive (NOA 61, Norland Products). The glass window was carefully placed over the craniotomy and, while maintaining a slight pressure, adhesive (Henkel Loctite 454) was used to secure the glass window to the surrounding skull. A stainless steel headplate was affixed on the skull with C&B Metabond (Parkell) centered on the glass window. Carprofen (5 mg/kg, s.c.) was given to the mouse immediately after surgery and on each

of the following 3 days. The mouse would recover for at least 10 days after the surgery before the start of imaging experiments.

Two-photon imaging

The two-photon microscope (Movable Objective Microscope, Sutter Instrument) was controlled by ScanImage 2020 software[21]. The laser excitation was provided by a tunable Ti:Sapphire femtosecond laser (Chameleon Ultra II, Coherent) and focused onto the mouse brain with a water-immersion 20X objective (XLUMPLFLN, 20x/0.95 N.A., Olympus). The laser power measured at the objective was ≤ 40 mW. To image GFP-expressing dendrites, the laser excitation wavelength was set at 920 nm, and a 475 – 550 nm bandpass filter was used to collect the fluorescence emission. During an imaging session, the mouse was head fixed and anesthetized with 1 – 1.5% isoflurane. Body temperature was controlled using a heating pad and DC Temperature Controller (40-90-8D, FHC) with rectal thermistor probe feedback. Each imaging session did not exceed 2 hours. We imaged apical tuft dendrites at 0 – 200 μm below the dura. To target Cg1/M2 region, we imaged within 0 – 400 μm of the midline as demarcated by the sagittal sinus. Multiple fields of view were imaged in the same mouse. For each field of view, 10 – 40-μm-thick image stacks were collected at 1 μm steps and at 1024 × 1024 pixels at 0.11 μm per pixel resolution.

For longitudinal imaging, we would return to the same fields of view across imaging sessions by locating and triangulating from a landmark on the left edge of the glass window. Each mouse was imaged on days -3, -1, 1, 3, 5 and 7 relative to the day of treatment. A subset of mice (2 males and 2 females) was imaged additionally on day 34. On the day of treatment (day 0), there was no imaging, and the mouse was injected with either psilocybin (1 mg/kg, i.p.) or saline (10 mL/kg, i.p.). After injection, the mouse was placed in a clean cage under normal room lighting to visually inspect for head-twitch responses for 10 minutes, before returning the mouse to its home cage.

Confocal imaging

Each mouse was injected with either psilocybin (1 mg/kg, i.p.) or saline (10 mL/kg, i.p.). At 24 hr after injection, the mouse was deeply anesthetized with isoflurane and transcardially perfused with phosphate buffered saline (PBS, P4417, Sigma-Aldrich) followed by paraformaldehyde (PFA, 4% in PBS). The brains were fixed in 4% PFA for 24 hours at 4 °C, and then 50-μm-thick coronal brain slices were sectioned using a vibratome (VT1000S, Leica) and placed on slides with coverslip with mounting medium. The brain slices were imaged with a confocal microscope (LSM 880, Zeiss) equipped with a Plan-Apochromat 63x/1.40 N.A. oil objective for dendritic spine imaging and a Plan-Apochromat 20x/0.8 N.A. objective for stitching images of an entire brain slice.

Analysis of the imaging data

Analyses of the two-photon and confocal imaging data were mostly similar, with an additional pre-processing step for motion correction of the two-photon imaging data using the StackReg plug-in[22] in ImageJ[23]. Structural parameters such as spine head width and spine protrusion length were quantified based on a standardized protocol[13, 18]. Briefly, if a protrusion extended for >0.4 μm from the dendritic shaft, a dendritic spine was counted. The head width of a dendritic spine was measured as the width at the widest part of the head of the spine. The protrusion length of a dendritic spine referred to the distance from its root at the shaft to the tip of the head. The line segment tool in ImageJ was used to measure the distances. Change in spine density, spine head width and spine protrusion length across imaging sessions were shown as fold-change from the value measured on the first imaging session (day -3) for each dendritic segment. The spine formation rate was calculated as the number of dendritic spines newly formed between two consecutive imaging sessions divided by the total number of dendritic spines observed in the first imaging session. The spine elimination rate was calculated as the number of dendritic spines lost between two consecutive imaging sessions divided by the total number of dendritic spines observed in the first imaging session. To assess the long-term dynamics of the spine formation and elimination rates across imaging sessions, we calculated the difference from the baseline rate, which was the spine formation or elimination rate of the same dendritic segment before psilocybin and saline injection (i.e., from day -3 to day -1). To quantify the persistence of newly formed spines, we calculated the number of dendritic spines newly formed on day 1 that are still present on day 7 and day 34, and divided by the total number of newly formed dendritic spines on day 1.

Statistics

Sample sizes and statistical analyses for each experiment are listed in **Supplementary Table 1**. Sample sizes were selected based on previous experiments reported in related publications[18, 24]. Animals were randomly assigned in the saline and psilocybin groups. No animals were excluded from data analysis. GraphPad Prism 8 and R were used for statistical analysis. In the figures, data are presented as the mean ± SEM per dendritic branch.

For *in vivo* two-photon imaging, dendritic spine scoring was performed while blind to treatment and time. Longitudinal measurements of dendrite structure were analyzed with mixed effects models for repeated measures using the *lme4* package in R. Linear mixed effects models were preferred to the commonly used repeated measures analysis of variance (ANOVA) due to fewer assumptions being made about the underlying data (e.g., balanced sampling, compound symmetry). Separate mixed effects models were created for each of five dependent variables: fold-change in spine density, fold-change in average spine head width, fold-change in average spine protrusion length, spine formation rate, and spine elimination rate. Each model included fixed effects for treatment (psilocybin vs. saline), sex (female vs. male), and time (Day 1, 3, 5, and 7) as factors, including all second and higher-order interactions between terms. Importantly, variation within mouse and dendrite across days was accounted by including random effects terms for dendrites nested by mice. Visual inspection of residual plots revealed no deviations from homoscedasticity or normality. *P*-values were calculated by likelihood ratio tests of the full model with the effect in question against the model without the effect in question. *Post hoc t*-tests were used to contrast psilocybin and saline groups per day, with and without splitting the sample by sex, applying Bonferroni correction for multiple comparisons. Spine persistence from two-photon imaging was analyzed with separate repeated measures ANOVAs for male and female mice, using fixed effects of treatment (psilocybin vs. saline), time (day 7 vs. day 34), and their interaction as independent predictors within dendrite.

For confocal imaging data, stricter blinding procedures involved one person performing imaging, another person scrambling the image file names, and a third person performing dendritic structural measurements blind to sex, treatment, and brain region. Data were unblinded after all of the measurements were completed. For each brain region in the confocal dataset (Cg1/M2, PrL/IL, and M1), separate two-way ANOVAs were constructed for apical and basal dendrites using spine density, spine head width, or spine protrusion length as the dependent variable. Treatment (psilocybin vs. saline), sex (female vs. male), and their interaction were included as independent predictors. *Post hoc t*-tests were used to contrast psilocybin and saline groups within sex, applying Bonferroni correction for multiple comparisons.

Data availability

The data that support the findings of this study will be made publicly available at https://github.com/Kwan-Lab.

Code availability

The code used to analyze the data in this study will be made publicly available at https://github.com/Kwan-Lab.

Acknowledgements

We thank B. Kelmendi and C. Pittenger for help on obtaining psilocybin, Usona Institute for providing psilocybin, J. Taylor for use of open-field activity boxes, H. Atilgan and H. Ortega for assistance on setting up video recording, and A. Halberstadt for advice on scoring head-twitch responses. This work was supported by the Yale Center for Psychedelic Science, NIH/NINDS training grant T32NS041228 (C.L.), and NIH/NIGMS Medical Scientist Training grant T32GM007205 (N.K.S.). We thank the Yale Center for Advanced Light Microscopy Facility for their assistance with confocal imaging, supported in part via NIH grant S10OD023598.

Author contributions

L.X.S. and A.C.K. designed the research. L.X.S. performed the two-photon and confocal imaging experiments, and analyzed the two-photon imaging data. N.K.S. blinded and I.G. analyzed the confocal imaging data. C.L. performed and analyzed the behavioral experiments. I.G. and K.D. assisted with analyzing the behavioral data. N.K.S. assisted with the statistical analyses. L.X.S. and A.C.K. wrote the paper, with input from all other authors.

Competing interests

A.C.K. received psilocybin from the investigational drug supply program at Usona Institute. The authors declare no other competing interests.

References

1. Vollenweider, F.X. & Preller, K.H. Psychedelic drugs: neurobiology and potential for treatment of psychiatric disorders. *Nat Rev Neurosci* **21**, 611-624 (2020).
2. Davis, A.K.*, et al.* Effects of Psilocybin-Assisted Therapy on Major Depressive Disorder: A Randomized Clinical Trial. *JAMA Psychiatry* (2020).
3. Carhart-Harris, R.L.*, et al.* Psilocybin with psychological support for treatment-resistant depression: an open-label feasibility study. *The Lancet Psychiatry* **3**, 619-627 (2016).
4. Nichols, C.D. & Sanders-Bush, E. A single dose of lysergic acid diethylamide influences gene expression patterns within the mammalian brain. *Neuropsychopharmacology* **26**, 634-642 (2002).
5. Vaidya, V.A., Marek, G.J., Aghajanian, G.K. & Duman, R.S. 5-HT2A receptor-mediated regulation of brain-derived neurotrophic factor mRNA in the hippocampus and the neocortex. *J Neurosci* **17**, 2785-2795 (1997).
6. Jones, K.A.*, et al.* Rapid modulation of spine morphology by the 5-HT2A serotonin receptor through kalirin-7 signaling. *Proc Natl Acad Sci U S A* **106**, 19575-19580 (2009).
7. Ly, C.*, et al.* Psychedelics Promote Structural and Functional Neural Plasticity. *Cell Rep* **23**, 3170-3182 (2018).
8. Cameron, L.P.*, et al.* A non-hallucinogenic psychedelic analogue with therapeutic potential. *Nature* (2020).
9. Halberstadt, A.L., Koedood, L., Powell, S.B. & Geyer, M.A. Differential contributions of serotonin receptors to the behavioral effects of indoleamine hallucinogens in mice. *J Psychopharmacol* **25**, 1548-1561 (2011).
10. Willins, D.L., Deutch, A.Y. & Roth, B.L. Serotonin 5-HT2A receptors are expressed on pyramidal cells and interneurons in the rat cortex. *Synapse* **27**, 79-82 (1997).
11. Jakab, R.L. & Goldman-Rakic, P.S. 5-Hydroxytryptamine2A serotonin receptors in the primate cerebral cortex: possible site of action of hallucinogenic and antipsychotic drugs in pyramidal cell apical dendrites. *Proc Natl Acad Sci U S A* **95**, 735-740 (1998).
12. Feng, G.*, et al.* Imaging neuronal subsets in transgenic mice expressing multiple spectral variants of GFP. *Neuron* **28**, 41-51 (2000).
13. Holtmaat, A.*, et al.* Long-term, high-resolution imaging in the mouse neocortex through a chronic cranial window. *Nat Protoc* **4**, 1128-1144 (2009).
14. Knott, G.W., Holtmaat, A., Wilbrecht, L., Welker, E. & Svoboda, K. Spine growth precedes synapse formation in the adult neocortex in vivo. *Nat Neurosci* **9**, 1117-1124 (2006).
15. Canal, C.E. & Morgan, D. Head-twitch response in rodents induced by the hallucinogen 2,5-dimethoxy-4-iodoamphetamine: a comprehensive history, a re-evaluation of mechanisms, and its utility as a model. *Drug Test Anal* **4**, 556-576 (2012).
16. Olson, D.E. The Subjective Effects of Psychedelics May Not Be Necessary for Their Enduring Therapeutic Effects. *ACS Pharmacology & Translational Science* (2020).
17. Yaden, D.B. & Griffiths, R.R. The Subjective Effects of Psychedelics Are Necessary for Their Enduring Therapeutic Effects. *ACS Pharmacology & Translational Science* (2020).
18. Phoumthipphavong, V., Barthas, F., Hassett, S. & Kwan, A.C. Longitudinal Effects of Ketamine on Dendritic Architecture In Vivo in the Mouse Medial Frontal Cortex. *eNeuro* **3**, ENEURO.0133-0115.2016 (2016).
19. Moda-Sava, R.N.*, et al.* Sustained rescue of prefrontal circuit dysfunction by antidepressant-induced spine formation. *Science* **364** (2019).
20. Savalia, N.K., Shao, L.-X. & Kwan, A.C. A Dendrite-Focused Framework for Understanding the Actions of Ketamine and Psychedelics. *Trends in Neurosciences*, in press (2020).
21. Pologruto, T.A., Sabatini, B.L. & Svoboda, K. ScanImage: flexible software for operating laser scanning microscopes. *Biomed Eng Online* **2**, 13 (2003).
22. Thevenaz, P., Ruttimann, U.E. & Unser, M. A pyramid approach to subpixel registration based on intensity. *IEEE Trans Image Process* **7**, 27-41 (1998).
23. Schneider, C.A., Rasband, W.S. & Eliceiri, K.W. NIH Image to ImageJ: 25 years of image analysis. *Nature Methods* **9**, 671-675 (2012).

24. Grutzendler, J., Kasthuri, N. & Gan, W.B. Long-term dendritic spine stability in the adult cortex. *Nature* **420**, 812-816 (2002).

Supplementary Figures

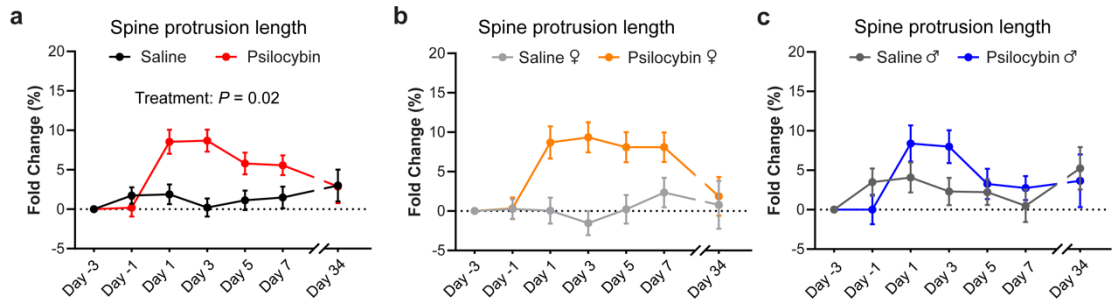

Supplementary Figure 1: Psilocybin increases spine protrusion length in Cg1/M2. (a) Effects of psilocybin or saline treatment on spine density in *Thy1*^{GFP} mice, plotted as fold-change from baseline value on Day -3. **(b, c)** Similar to (a), plotted separately for females and males. **(j – l)** Similar to (g – i) for spine head width. Mean ± SEM. Sample sizes and statistical analyses are provided in Supplementary Table 1.

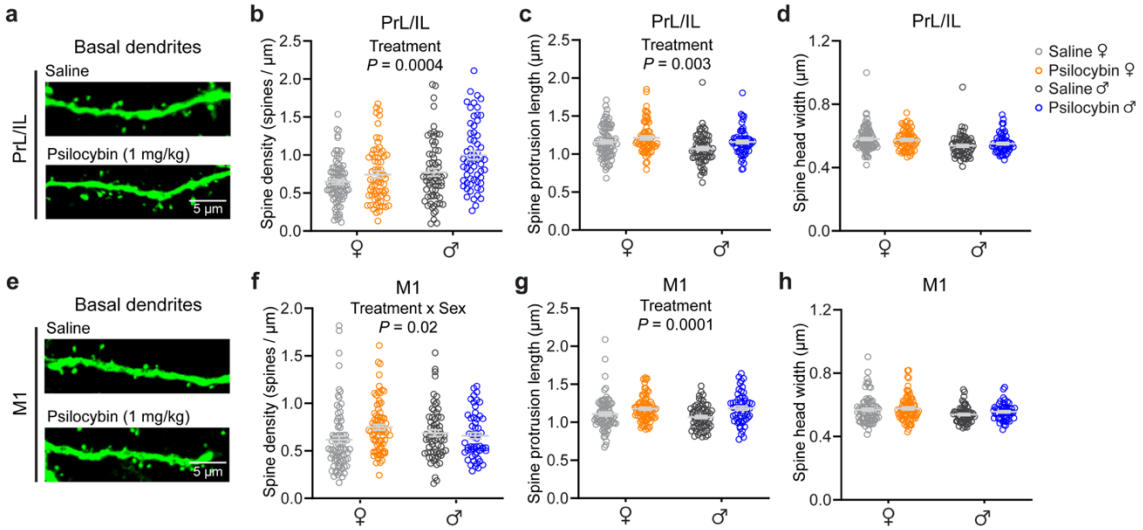

Supplementary Figure 2. Effects of psilocybin on basal dendrites in PrL/IL and M1. (a) Images of basal dendritic segments in PrL/IL from coronal brain sections from a *Thy1*^{GFP} mouse. **(b)** Effects of psilocybin and saline on spine density for basal dendrites in PrL/IL. Open circles, individual dendritic segments. **(c)** Similar to (b) for spine protrusion length. **(d)** Similar to (b) for spine head width. **(e – h)** Similar to (a – d) for M1. Mean, SEM. Sample sizes and details of the ANOVA models are provided in Supplementary Table 1.